Development/Plasticity/Repair

Gas6 Deficiency Increases Oligodendrocyte Loss and Microglial Activation in Response to Cuprizone-Induced Demyelination

Michele D. Binder,[1,2] Holly S. Cate,[1,2] Anne L. Prieto,[3] Dennis Kemper,[1] Helmut Butzkueven,[1,2] Melissa M. Gresle,[1,2] Tania Cipriani,[1] Vilija G. Jokubaitis,[1] Peter Carmeliet,[4] and Trevor J. Kilpatrick[1,2]

[1]Howard Florey Institute and [2]The Centre for Neuroscience, University of Melbourne, Parkville, Victoria 3010, Australia, [3]Department of Psychological and Brain Sciences, Indiana University, Bloomington, Indiana 47405, and [4]Flanders Interuniversitary Institute for Biotechnology, University of Leuven, B-3000 Leuven, Belgium

The TAM family of receptor protein tyrosine kinases comprises three known members, namely Tyro3, Axl, and Mer. These receptors are widely expressed in the nervous system, including by oligodendrocytes, the cell type responsible for myelinating the CNS. We examined the potential role of the TAM family and of their principle cognate ligand, Gas6 (growth arrest gene 6), in modulating the phenotype of the cuprizone model of demyelination. We found that the expression profiles of *Axl*, *Mer*, and *Gas6* mRNA were increased in the corpus callosum in a temporal profile correlating with the increased migration and proliferation of microglia/macrophages in this model. In contrast, expression of *Tyro3* decreased, correlating with the loss of oligodendrocytes. Gas6 both promoted *in vitro* survival of oligodendrocytes (39.3 ± 3.1 vs 11.8 ± 2.4%) and modulated markers of activation in purified cultures of microglia (tumor necrosis factor α mRNA expression was reduced ~48%). In Gas6$^{-/-}$ mice subjected to cuprizone-challenge, demyelination was greater than in control mice, within the rostral region of the corpus callosum, as assessed by luxol fast blue staining (myelination reduced by 36%) and by ultrastructural analysis. An increased loss of Gst-π (glutathione *S*-transferase-π)-positive oligodendrocytes was also identified throughout the corpus callosum of Gas6$^{-/-}$ mice. Microglial marker expression (ionized calcium-binding adapter molecule 1) was increased in Gas6$^{-/-}$ mice but was restricted to the rostral corpus callosum. Therefore, TAM receptor activation and regulation can independently influence both oligodendrocyte survival and the microglial response after CNS damage.

Key words: **Gas6; oligodendrocytes; microglia; demyelination; TAM receptor; cuprizone**

Introduction

Oligodendrocyte damage and death are common elements of CNS demyelination (Barnett and Prineas, 2004). One potential strategy for preventing or ameliorating demyelination is to inhibit the death of damaged oligodendrocytes. Previous work in our laboratory has focused on using microarray strategies to identify factors important in oligodendrocyte survival during demyelination. Using this strategy, we identified the TAM receptor family as potentially important.

The TAM family of receptor protein tyrosine kinases comprises three known members, Tyro3, Axl, and Mer, first identified by Lai and Lemke (1991), and shown to be widely expressed in the nervous system, including oligodendrocytes (Prieto et al., 2000, 2007). Recent work using various knock-outs of these receptors has demonstrated that they play an essential role in the reproductive, nervous, and immune systems (Lu et al., 1999; Lu and Lemke, 2001). Two ligands are known for the TAM receptors, Gas6 (growth arrest gene 6) and the structurally related protein S (Stitt et al., 1995; Nagata et al., 1996; Prasad et al., 2006). To date, the function of Gas6 as a ligand for the TAM receptors has been better studied than protein S. In particular, Gas6 has been shown to have both mitogenic and survival activities for a variety of cell types, including neurons, Schwann cells, and human and mouse oligodendrocytes (Li et al., 1996; Yagami et al., 2002; Shankar et al., 2003, 2006).

In addition to oligodendrocyte loss, demyelinating diseases such as multiple sclerosis often have an inflammatory component that may exacerbate or, in some circumstances, ameliorate the symptoms of disease (for review, see Raivich and Banati, 2004). Brain-resident microglia, along with peripheral macrophages, are activated in various CNS disorders, including infection, neurodegeneration, stroke, and autoimmune disorders such as multiple sclerosis. Activated microglia secrete a variety of proteins, including cytokines and reactive oxygen species, which can ultimately damage oligodendrocytes. Additionally, microglia

Received July 20, 2007; accepted April 4, 2008.

This work was supported by the Multiple Sclerosis Research Australia, the National Health and Medical Research Council of Australia (NH&MRC), and in part by National Institutes of Health Grant NS37471 (A.L.P.) and the Indiana METACyt Initiative of Indiana University, funded through a major grant from the Lilly Endowment (Indianapolis, IN). H.S.C. was supported by the NH&MRC through the award of a Peter Doherty Fellowship. H.B. was supported by a Betty Cuthbert Fellowship from the NH&MRC and by the Multiple Sclerosis Research Australia. We thank Dr. Patrick Jones for provision of purified recombinant Gas6 and Faye Doherty and Catherine Chang for technical support.

Correspondence should be addressed to Trevor J. Kilpatrick, Howard Florey Institute, University of Melbourne, Victoria 3010, Australia. E-mail: t.kilpatrick@hfi.unimelb.edu.au.

DOI:10.1523/JNEUROSCI.1180-08.2008

 0270-6474/08/285195-12$15.00/0

can secrete trophic factors, which could support damaged cells and induce repair.

In the cuprizone model of demyelination, there is a large recruitment of microglia/macrophages both before and during demyelination (Hiremath et al., 1998; McMahon et al., 2002). There is activation and proliferation of microglia and some infiltration of peripheral macrophages (McMahon et al., 2002). Although the exact role of microglia/macrophages in cuprizone-induced demyelination is uncertain, it seems clear they play dichotomous roles, influencing both demyelination and remyelination.

Given the known role that TAM receptors and Gas6 play in regulating both cell survival and immune function, we examined the role of these molecules in oligodendrocyte survival *in vitro* and in cuprizone-induced demyelination. We demonstrate that Gas6 is a potent survival factor for oligodendrocytes *in vitro*. Additionally, we demonstrate that the TAM receptors are regulated in purified activated microglia and that administration of exogenous Gas6 can modulate microglial activation. Using Gas6 knock-out mice, we further show that in the absence of Gas6, demyelination is exacerbated and microglial activation is increased. These results provide evidence that Gas6 and its receptors play an important role in supporting oligodendrocyte survival and modulating immune activity during a demyelinating insult.

Materials and Methods

Animals and reagents. Sprague Dawley rats and C57BL/6 mice were obtained from the Animal Resource Centre (Canning Vale, Western Australia, Australia). Gas6$^{-/-}$ mice were backcrossed onto the C57BL/6 background. All animal experiments were conducted according to National Health and Medical Research Council guidelines.

All chemicals were obtained from Sigma-Aldrich (St. Louis, MO) unless otherwise indicated. Recombinant human Gas6 (rhGas6) was a kind gift from Dr. Patrick Jones (Berlex Biosciences, Richmond, CA). All cell culture plasticware was purchased from Nalge Nunc International (Rochester, NY). All cell culture media and reagents were purchased from Invitrogen (Carlsbad, CA) unless otherwise noted. All secondary antibodies were purchased from Jackson ImmunoResearch Laboratories (West Grove, PA) unless otherwise noted.

Purification and culture of rat oligodendrocyte precursor cells. Oligodendrocyte precursor cells (OPCs) were purified from the optic nerve of postnatal day 7 (P7) rats as described previously (Barres et al., 1992). Purified cells were cultured in 25 cm^2 tissue culture flasks coated with poly-D-lysine (PDL) in modified Bottenstein-SATO medium (Bottenstein and Sato, 1979) containing *N*-acetyl-cysteine (60 μg/ml), forskolin (5 μM), penicillin and streptomycin, NT-3 (5 ng/ml; Peprotech, Rocky Hill, NJ), and PDGF-A chain homodimer (10 ng/ml; Peprotech). For RNA preparation, cells were cultured in 10 cm PDL-coated dishes to a density of $\sim 1 \times 10^6$ cells per dish. In some experiments, TH (3,5,3-triiodo-L-thyronine; 40 ng/ml) was added to the culture medium, according to the experimental paradigm.

Purification and culture of rat microglia. Mixed glial cell cultures were prepared from the cortices of P2 rat brains using differential adhesion to plastic as described previously (McCarthy and de Vellis, 1980; Li et al., 2003) with modifications. Briefly, rats were decapitated and brains removed to HBSS containing 1 mM sodium pyruvate, 3.9 mM glucose, and 10 mM HEPES. The meninges were removed, and cortices were isolated, minced, and then digested in 0.015% trypsin (w/v) (Roche Applied Science, Indianapolis, IN). Trypsin reaction was stopped with 0.05% trypsin inhibitor (w/v) (Roche Applied Science), and cells were briefly centrifuged and then resuspended in DMEM/5% fetal calf serum (FCS) and triturated to a single-cell suspension. Cells were plated in PDL-coated 75 cm^2 tissue culture flasks and cultured at 37°C/5% CO_2. Media was changed on days 1 and 4 of culture. Microglia were collected on day 7 by vigorously tapping flasks and collecting supernatant. Cells were briefly centrifuged and resuspended in culture media. The glial conditioned media (GCM) from the mixed culture was collected and used for initial culture of microglia. Microglia were cultured on 10 cm^2 tissue culture dishes for 24 h in 50% GCM/50% modified Bottenstein-SATO to allow cells to quiesce and ramify before use in experiments. After 24 h, media were replaced with modified Bottenstein-SATO/0.5% FCS, and cells were cultured at 37°C/8% CO_2. For assessment of microglial proliferation, cells were cultured in slide flasks in the presence or absence of Gas6, according the experimental paradigm.

Bromodeoxyuridine incorporation. To label cells in S-phase, bromodeoxyuridine (BrdU) (10 μM) was added to the culture medium for 17 h (OPCs) or 24 h (microglia). Cells were then fixed in 4% paraformaldehyde for 5 min. After washing, the DNA was denatured in 2 M HCl for 15 min, followed by neutralization in 0.1 M sodium borate for 15 min. Cells were then washed and permeabilized with 20% normal goat serum/0.4% Triton X-100 for 30 min. The cells were incubated with a monoclonal anti-BrdU antibody (1:40; GE Healthcare, Little Chalfont, Buckinghamshire, UK) for 1 h, followed by a goat anti-mouse IgG conjugated with FITC (1:500) for 30 min. The final antibody incubation included Hoescht 33342 (1:2000; Invitrogen) to visualize the nucleus of all cells. For all assays, six wells were counted and assays were performed at least three times with independent cell isolations. All results are expressed as percentage of BrdU+ cells ± SEM. Statistical significance was determined using one-way ANOVAs with Bonferroni's *post hoc* multiple comparison tests.

Determination of cell death. OPCs were differentiated for 48 h in the absence of mitogens. Oligodendrocytes were then plated onto PDL-coated coverslips at a density of ~150 cells per well in 24-well plates. Cells were cultured in modified Bottenstein-SATO medium (in the absence of insulin) with appropriate factors according to the experimental paradigm for 48 h. Ethidium homodimer-1 (4 mM; Invitrogen) and calcein AM (4 mM; Invitrogen) were added to each well. Cells were then visualized on an inverted fluorescent microscope (Carl Zeiss, Thornwood, NY) and live (calcein AM positive) and dead (ethidium homodimer-1 positive) cells counted. For all assays, six wells were counted, and assays were repeated at least two times with independent cell isolations. All results are expressed as percentage of live cells ± SEM. Statistical significance was determined using one-way ANOVAs with Bonferroni's *post hoc* multiple comparison tests.

Quantitative PCR. All quantitative PCR (qPCR) was performed on an ABI7700 sequence detection system (Applied Biosystems, Foster City, CA) using the comparative Ct method (Livak and Schmittgen, 2001). All primers were designed using Primer Express 1.5 (Applied Biosystems). Sequences of primers were as follows: mouse and rat 18S, forward 5′CGGCTACCACATCCAAGGAA3′, reverse 5′GCTGGAATTACCGCGGCT3′; rat Axl forward 5′TATGCCCTGATGTCCCGGT3′, reverse 5′TCCCGGAGCTCTGCAAAAC3′; mouse Axl forward 5′TCTAATGTTGGCCTGATCTTCGT3′, reverse 5′GCCTCTTGTGACTTAGATGCTGAG3′; rat Gas6 forward 5′ACCACTCCACAAAGAAGCTCAAG3′, reverse 5′GGGCCAGGGCAACATTC3′; mouse Gas6 forward 5′GCTGCAGCTTCGGTACAATG3′, reverse 5′ACATGCCGTGGTTGATGGTT3′; rat interleukin 1β (IL1β) forward 5′AGGCTTCCTTGTGCAAGTG3′, reverse 5′TCGAAAGCTGCTATTTCACAGTTG3′; rat inducible nitric oxide synthase (iNOS) forward 5′CCCCCTTCCGAAGTTTCTG3′, reverse 5′GCCTCCTTTGAGCCCTCTGT3′; rat Mer forward 5′TCTCCACAGGGATTTAGCTGC3′, reverse 5′AGGCCAAAGTCTGCCACG3′; mouse Mer forward 5′TTGCGGGATGACATGACTGT3′, reverse 5′CGGTAATAATCACCACTGTAAATCTTTCT3′; rat Tyro3 forward 5′TTCCCGACCAGCCATTATTC3′, reverse 5′TCGTTGTTACTGTGATGTTGAAAGG3′; mouse Tyro3 forward 5′TGGCTGAGCTGCTCCTACTTTA3′, reverse 5′TGGGCAGTGCTGAGTTCCA3′; rat tumor necrosis factor α (TNFα) forward 5′ACAAGGCTGCCCCGACTAC3′, reverse 5′TCCTGGTATGAAATGGCAAACC3′; rat CD11b forward 5′AAGGTCATACAGCATCAGTACCAGTT3′, reverse 5′TCCAGAAGACCACGCTGACA3′; mouse Mac1/CD11b forward 5′AAGTGGAGCCATATGAAGTTCACA3′, reverse 5′GCACCAGGCCCCCAAT3′; mouse CD68 forward 5′GGACTACATGGCGGTGGAATA3′, reverse 5′GATGAATTCTGCGCCATGAA3′; mouse myelin basic protein (MBP) forward 5′CCCGTGGAGCCGTGATC3′, reverse 5′TCTTCAAACGAAAAGGGACGAA3′.

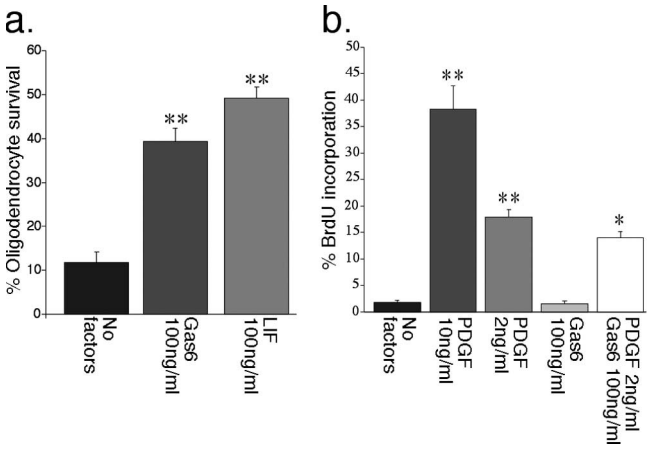

Figure 1. rhGas6 increases oligodendrocyte viability but not proliferation *in vitro*. ***a***, Purified mature oligodendrocytes were plated at a density of 150 cells/well in SATO in the presence or absence of either rhGas6 or LIF. Cells were cultured for 48 h and then assessed for viability using calcein AM/ethidium homodimer-1. Six wells were counted per condition. Viability is expressed as a percentage of total cell number. Both LIF and Gas6 significantly increased the viability of cultured oligodendrocytes (**$p < 0.001$). ***b***, Purified OPCs were plated at a density of 150 cells per well in SATO in the presence or absence of growth factors as specified and cultured for 48 h. BrdU was added for the final 17 h of culture. Cells were fixed and stained for BrdU, and the number of positive cells was counted. Results are expressed as a percentage of BrdU-positive cells per total cells counted (*$p < 0.01$, **$p < 0.001$, compared with no factors).

cDNA was prepared from 0.5 μg of RNA using the Taqman Reverse Transcription reagents (Applied Biosystems), according to manufacturer instructions, and used at a dilution of 1:20. SYBR green (Applied Biosystems) was used to determine relative Ct values according to manufacturer instructions. All reactions were run as single-plex reactions and the $2^{-\Delta\Delta CT}$ value expressed relative to 18S (Livak and Schmittgen, 2001). All changes are shown as relative expression values. In the absence of ribosomal RNA, relative expression from amplified RNA samples was determined using the $2^{-\Delta CT'}$ method (Livak and Schmittgen, 2001). All relative expression values are expressed as ± SD. To determine statistical significance, confidence intervals were constructed where appropriate for single-variate analysis. For multivariate comparisons, either one-way or two-way ANOVAs with Bonferroni's *post hoc* multiple comparison tests were performed.

Induction of demyelination. Cuprizone-mediated demyelination was induced by feeding 8-week-old mice powdered feed (Barastoc, Pakenham, Victoria, Australia) containing 0.2% cuprizone (w/w, biscyclohexanone-oxaldihydrazone) for up to 6 weeks, according to the experimental paradigm. Feed was refreshed each day. Wild-type littermates were used as controls for induction of demyelination in Gas6$^{-/-}$ cohorts. In one cohort (cohort 1), the wild-type control animals were supplemented with separately bred C57BL/6 mice to increase available numbers. In total, an equal mix of male and female wild-type and Gas6$^{-/-}$ mice were subjected to cuprizone challenge with no gender effect identified. Cohort 1 was embedded, cut, and analyzed in the coronal orientation, and cohort 2 was embedded, cut, and analyzed in sagittal orientation.

Laser capture microdissection. Tissue from the corpus callosum of cuprizone-challenged mice was microdissected using the PALM microbeam/microlaser system (Carl Zeiss) as described previously (Emery et al., 2006).

Histology. Mice were anesthetized and perfused intracardially with PBS followed by 4% paraformaldehyde, and the brains were embedded in paraffin or, for cryosectioning, were equilibrated successively in 12, 16, and 18% sucrose in PBS for cryoprotection and then frozen in dry ice. Cryostat sections (15 μm) were collected onto chrom-alum-coated slides. For coronal analysis, paraffin sections were selected from appropriate regions of the brain: rostral sections were as close to Bregma 0.38 as the series of sections would allow; middle from Bregma −0.70; and caudal from Bregma −0.94 (Paxinos and Franklin, 2001). Sagittal paraffin sections (10 μm) were selected as close to lateral 0.12 mm as the series of sections would allow (Paxinos and Franklin, 2001), with adjacent sections proceeding further laterally as required. Myelination in cuprizone-challenged animals was assessed using luxol fast blue (LFB)-periodic acid Schiff reagent using paraffin-embedded sections. Quantification of LFB staining was as described below.

For electron microscopic evaluation of myelin, mice were perfused as above and processed for resin embedding. Semithin sections (0.5 μm) were cut to evaluate quality and orientation. Representative samples were then chosen, and ultrathin sections (90 nm) were cut and images captured using a Siemens Stereoskop Transmission Electron Microscope (Siemens, Munich, Germany) at 3000× magnification. Quantification of myelinated axons was determined using methylene blue staining of semithin sections (0.5 μm) of the rostral portion of the corpus callosum corresponding to approximately Bregma 0.38. Images were captured using a Carl Zeiss Axioplan microscope and overlaid with a grid. Two grids of equal size corresponding to 249 μm^2 were counted for each animal and averaged. Counts are expressed as the number of myelinated axons/mm^2 ± SEM. Statistical significance was determined using Student's *t* test with unequal variances.

Immunohistochemistry and immunofluorescence. Paraffin sections were prepared as described above. For DAB immunohistochemistry, detection of Axl and Mer antigens was based on the method of Wang et al. (2005) using goat anti-Axl (1:400; Santa Cruz Biochemicals, Santa Cruz, CA) and goat anti-Mer (1:400; Santa Cruz Biochemicals). Primary antibody was detected using a the VectaStain Elite ABC kit (Vector Laboratories, Burlingame, CA) with DAB as a substrate (Vector Laboratories) and counterstained with hemotoxylin (Vector Laboratories). Detection of ionized calcium-binding adapter molecule 1 (IBA1) was as for Axl and Mer, with the exception that antigen was retrieved using 0.05 M Tris, pH 7.6/1.5% NaCl for 7 min at 100°C. Anti-IBA1 (Wako Pure Chemicals, Tokyo, Japan) was used at 1:1000. Sections for image analysis (see below) were not counterstained with hemotoxylin. Double immunohistochemistry for Axl or Mer with IBA1 was performed as for single Axl and Mer staining but extended as follows. After primary antibody binding was detected using DAB substrate, the sections were washed in PBS and incubated overnight in 1:1000 anti-IBA1. Detection of primary antibody binding was performed using a VectaStain ABC-AP kit (Vector Laboratories) with alkaline phosphatase (VectaBlue) as a substrate (Vector Laboratories).

Immunofluorescence staining was used to detect the glutathione *S*-transferase (GST) π isoform (Gst-Pi) in paraffin-embedded sections. Sections were rehydrated as for DAB immunohistochemistry, and antigen was retrieved by incubation at 95°C for 40 min in 10 mM citric acid buffer (pH 6.0)/0.05% Tween 20. Blocking [1 h at room temperature (RT)] and subsequent antibody incubations were performed in 10% normal goat serum/0.1% BSA/0.3% Triton X-100. Sections were incubated with rabbit anti-GST3 (1:300; Abcam, Cambridge, MA) overnight at RT followed by goat anti-rabbit IgG-conjugated with biotin (Vector Laboratories). Antibody was detected by incubation with Fluorescein Avidin D (1:200; Vector Laboratories). The final antibody incubation included Hoescht 33342 (1:2000; Invitrogen) to visualize the nucleus of all cells.

To detect the expression of Tyro3, cryosections were prepared as described above and blocked for 1 h with blocking buffer consisting of 5% goat serum (Colorado Serum, Denver, CO), 5% FCS (Omega Scientific, Tarzana, CA), PBS, and 0.1% Triton X-100. Before staining, the fixed sections were washed three times with PBS for 10 min each. The #2792 serum against Tyro3 (1:200) (Prieto et al., 2000) or 2′, 3′-cyclic nucleotide 3′-phosphodiesterase (CNPase) antibody (Covance Research Products, Berkeley, CA) or the preabsorbed serum was diluted in blocking buffer, applied to the tissue sections, and incubated overnight at 4°C. The sections were then washed five times for 5 min each in 1% goat serum and PBS and blocked as above for 30 min. The tissue sections were incubated for 60 min with Alexa 488-labeled goat anti-rabbit antibodies (for the anti-Tyro3 antibodies) and Alexa 594-labeled goat anti-mouse antibodies (1:200 dilution) for the CNPase antibodies. The sections were washed five times for 5 min washes in PBS/1% goat serum and were mounted using Vectashield (Vector Laboratories).

Quantification of LFB and IBA1 staining. Image analysis of LFB-stained sections was conducted using NIH Image 1.63 according to procedures described previously (Emery et al., 2006). All images from a given experiment were acquired in a single session using the same light intensity and filter settings. In addition, the white balance of all images was standardized to eliminate color bias. Density measurements are shown as raw mean intensities ± SEM. The area of the corpus callosum was determined using the NIH Image software 1.63 and converting areas to squared millimeters. The level of IBA1 reactivity was measured using mean intensity of DAB staining. Images corresponding to the rostral, middle, and caudal regions of the corpus callosum were obtained. The yellow channel of each image was extracted, and the images were converted to grayscale. The mean density of staining in each region was determined using NIH Image 1.63, and the mean density of a cortical area immediately dorsal to the corpus callosum was also measured. Final mean densities are expressed as (corpus callosum mean density − cortex mean density) ± SEM. Statistical significance was determined using two-way ANOVA with Bonferroni's *post hoc* tests for multiple comparisons.

Quantification of microglia and oligodendrocyte number. To quantify the number of microglia, coronal sections were stained with IBA1 as described above. Rostral images were captured from approximately Bregma 0.14 mm and caudal images from approximately Bregma −1.06 mm. Images were captured using a Carl Zeiss Axioplan microscope with a 40× objective, and the same light intensity and filters were used for all images. Images from three adjacent sections were captured for each individual animal. The density of cells in this area was quite high; therefore, to enable quantification, each image was overlaid with a grid, and two grids of equal size were counted within the image. Both the number of IBA1-immunoreactive cells and the total cell number was determined. The area of each grid was determined, and cell counts were expressed as the number of IBA1-positive cells/mm^2. All results are expressed as mean IBA1-positive cells ± SEM. Statistical significance was determined using two-way ANOVA with Bonferroni's *post hoc* tests for multiple comparisons.

To quantify the number of oligodendrocytes, coronal sections were stained with Gst-π as described above. Images were captured from the same regions as described above for IBA1 quantification using a Carl Zeiss Axioplan microscope with a 20× objective. All cells in the corpus callosum contained within the 20× image were counted. The area of the corpus callosum was determined using NIH ImageJ v1.38. All results are expressed as number of Gst-π-positive cells/mm^2. Statistical significance was determined using two-way ANOVA with Bonferroni's *post hoc* tests for multiple comparisons.

Statistical analysis. All statistical tests were performed using GraphPad Prism (GraphPad Software, San Diego, CA). Individual statistical tests were performed as described in the relevant sections. For all quantification of cell number or myelination status, all analyses were performed by an investigator blind to both the treatment and genotype of the animal.

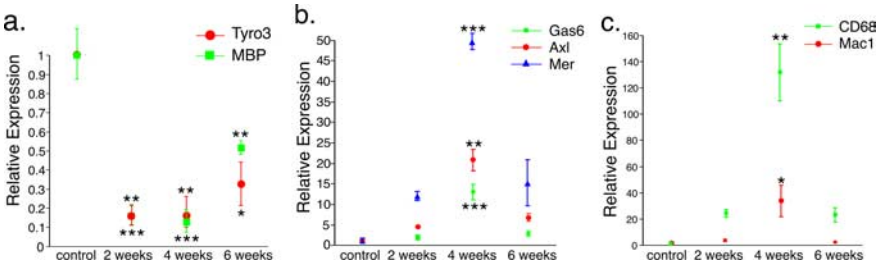

Figure 2. TAM receptor and Gas6 gene expression profiles are regulated during demyelination. ***a–c***, The corpus callosum of unchallenged mice or mice challenged with cuprizone for 2, 4, or 6 weeks ($n = 2$ for each time point) was collected, and mRNA levels were measured using qPCR. ***a***, *Tyro3* and *MBP* mRNA expression profiles were significantly reduced at all time points examined (*$p < 0.05$, **$p < 0.01$, ***$p < 0.001$, compared with unchallenged mice). ***b***, *Gas6*, *Axl*, and *Mer* mRNA expression profiles were significantly increased at 4 weeks of cuprizone challenge (**$p < 0.01$, ***$p < 0.001$). ***c***, *CD68* and *CD11b* mRNA expression profiles were significantly increased at 4 weeks of cuprizone challenge (*$p < 0.05$, **$p < 0.01$).

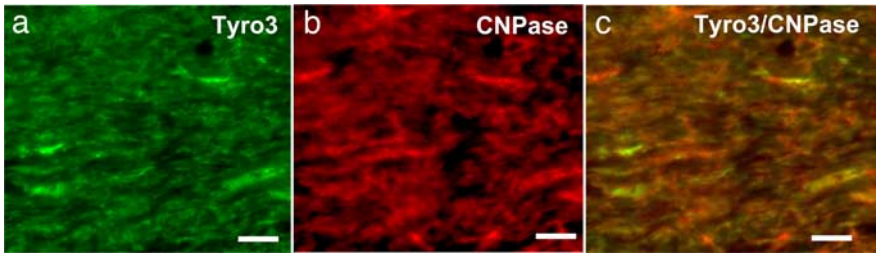

Figure 3. Tyro3 expression in oligodendrocytes of the corpus callosum. ***a***, ***b***, Coronal sections (15 μm) of 8 week mouse brains were double stained with anti-Tyro3 serum (***a***, green) and anti-CNPase (***b***, red) to label oligodendrocytes. ***c***, Tyro3 was detected in oligodendrocytes as revealed by the yellow regions indicating overlap in the staining of Tyro3 and cell type-specific antibodies. Scale bar, 20 μm.

Results

Gas6 is a survival factor, but not a mitogen, for rat oligodendrocytes *in vitro*

We initially investigated the influence of Gas6 on purified oligodendrocytes isolated from the postnatal rat optic nerve. In the presence of 100 ng/ml rhGas6, after 48 h in culture, 39.3 ± 3.1% oligodendrocytes remained viable compared with 11.8 ± 2.4% in the basal condition ($p < 0.001$) (Fig. 1*a*). The increased viability seen in the presence of rhGas6 was of a similar order to that seen in the presence of leukemia inhibitory factor (LIF) (49.1 ± 2.6%) (Fig. 1*a*), a known survival factor for rat oligodendrocytes (Barres et al., 1993). The survival effect of rhGas6 peaked at 100 ng/ml (supplemental Fig. 1, available at www.jneurosci.org as supplemental material), and all additional experiments used this concentration of rhGas6.

It has been shown previously in other cell types that Gas6 can act as a mitogen. To assess whether this mitogenic effect also applied to rat OPCs, we cultured OPCs with Gas6 in the presence or absence of PDGF at 2 ng/ml, because this represented the ED_{50} value for the induction of proliferation by this mitogen in these cells (Barres et al., 1993). The proliferative index was determined by calculating the percentage of BrdU-positive cells. As illustrated in Figure 1*b*, compared with no growth factors, Gas6 alone did not increase the number of BrdU-positive cells (1.2 ± 0.5 and 1.0 ± 0.4%, with or without Gas6, respectively; $p > 0.05$). Additionally, in the presence of 2 ng/ml PDGF, Gas6 did not further increase the rate of BrdU incorporation (17.7 ± 3.6 and 14.0 ± 2.7%; $p > 0.05$, with or without Gas6, respectively). These results indicate that Gas6 does not act as a mitogen for rat oligodendrocytes *in vitro*.

Gas6 and its receptors are regulated in a mouse model of demyelination

We next examined the serial expression of *Gas6* and its receptors in a mouse model of demyelination, the toxic cuprizone model. Using qPCR, expression of the *Tyro3* gene decreased during cuprizone-induced demyelination. As shown in Figure 2*a*, *Tyro3* gene expression decreased 6.5-fold ($p < 0.01$) and 8.5-fold ($p < 0.01$) after 2 and 4 weeks of cuprizone challenge, respectively. After 6 weeks of cuprizone challenge, *Tyro3* gene expression re-

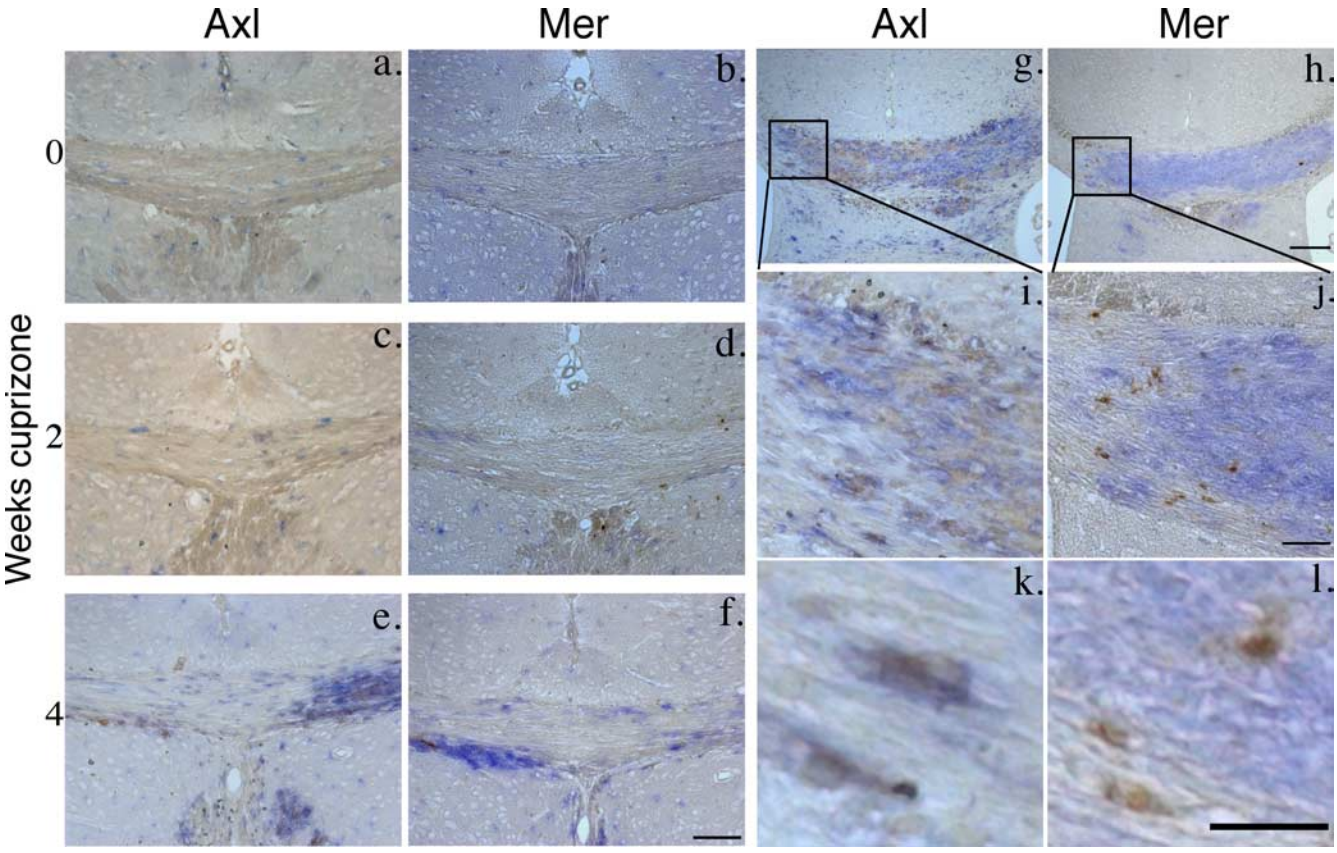

Figure 4. Microglia upregulate Axl and Mer in response to cuprizone challenge. ***a–f***, Double-immunoperoxidase staining for Axl and Mer (brown) and IBA1 (blue) in the midline corpus callosum of unchallenged mice or mice challenged with cuprizone for 2 or 4 weeks ($n = 4$ for each time point). ***a***, ***b***, In unchallenged animals, a small number of IBA1-positive cells, evenly distributed throughout the corpus callosum, was observed. At this time point, cells positive for either Axl (***a***) or Mer (***b***) were rarely observed. ***c***, ***d***, After 2 weeks of cuprizone challenge, a small increase in the number of IBA1-positive cells was observed. ***k***, ***l***, Some of the IBA1-positive cells were also positive for Axl (***k***) or Mer (***l***). Cells positive for Axl or Mer alone were rarely observed. ***e***, ***f***, After 4 weeks of cuprizone challenge, the number of IBA1-positive cells in the corpus callosum was greatly increased, with a concomitant increase in Axl (***e***) and Mer (***f***) immunoreactivity among IBA1-positive cells, although Mer reactivity appeared less extensive. ***g***, ***h***, The dissociation between Axl- and Mer-positive cells is shown in staining of adjacent sections from mice challenged with cuprizone for 4 weeks. ***g–j***, Axl positivity (***g***, ***i***) appears to extend throughout the region of IBA1 expression, whereas Mer appears restricted to a subset of IBA1-positive microglia (***h***, ***j***). Scale bars: ***a–f***, ***i***, ***j***, 100 μm; ***g***, ***h***, 200 μm; ***k***, ***l***, 50 μm.

mained significantly reduced compared with untreated control mice ($p < 0.05$) but increased compared with the 2 and 4 week time points, although this increase did not reach significance ($p > 0.05$). We also assessed the expression profile of the gene encoding *MBP*, a myelin marker, and found that, like *Tyro3*, its expression was significantly reduced after 2 and 4 weeks of cuprizone challenge ($p < 0.001$) (Fig. 2*a*) with an increase in *MBP* at 6 weeks, although still below baseline levels ($p < 0.01$). This pattern correlates well with the previous reports of demyelination peaking at 4–5 weeks of cuprizone challenge, with some spontaneous remyelination at 6 weeks (Matsushima and Morell, 2001).

In contrast to *Tyro3* gene expression, expression profiles of the genes encoding the *Axl* and *Mer* receptors and of Gas6 were increased after 2 and 4 weeks of cuprizone challenge compared with unchallenged controls. The increase in expression of all three genes peaked at 4 weeks of cuprizone challenge, with *Gas6* increasing 12.9-fold ($p < 0.001$), *Axl* increasing 20.6-fold ($p < 0.01$), and *Mer* increasing 40.7-fold ($p < 0.01$) over unchallenged controls (Fig. 2*b*). At 6 weeks of cuprizone challenge, the level of expression of transcripts for all three genes was significantly reduced compared with the 4 week level (*Gas6*, $p < 0.001$; *Axl*, $p < 0.05$; *Mer*, $p < 0.01$) and was no longer significantly different from unchallenged controls ($p > 0.05$). This pattern of expression coincides with the increase in microglial migration and proliferation previously shown to occur during cuprizone-induced demyelination (Matsushima and Morell, 2001). In support of this view, we found that expression profiles of the genes encoding the microglia/macrophage markers *CD68* and *CD11b* were increased after 2 weeks of cuprizone challenge (3.3-fold and 24.1-fold, respectively), peaking at 4 weeks, when expression was significantly different from unchallenged controls (*CD11b* increased 31.5-fold, $p < 0.05$; *CD68* increased 130.0-fold, $p < 0.01$). The expression of the *CD68* and *CD11b* genes then reduced to a lower level at 6 weeks (1.9-fold and 22.4-fold, respectively) with transcript levels no longer significantly different from unchallenged controls (Fig. 2*c*).

Next, we examined the regulation of the Tyro3, Axl, and Mer receptors at the protein level using immunohistochemistry. Using standard immunohistochemical methods, we were unable to detect the presence of Tyro3 in the corpus callosum of either healthy or cuprizone-challenged mice. However, using frozen sections, we were able to determine that the Tyro3 protein was expressed by cells in the corpus callosum of healthy mice (Fig. 3*a*), some of which colocalize with CNPase, a marker for mature oligodendrocytes (Fig. 3*b*,*c*). However, consistent with downregulated *Tyro3* gene expression in cuprizone-challenged mice (Fig. 2*a*), we could not identify Tyro3 protein expression in this context.

Because the expression of both the Axl and Mer genes coincided with an increase in microglial activation, we also undertook

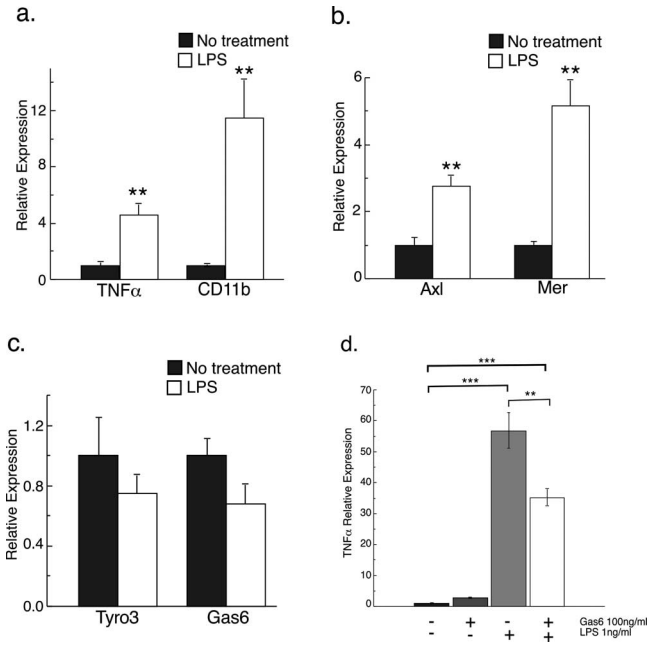

Figure 5. The expression profiles of TAM receptors and Gas6 mRNA are regulated in response to microglial activation, and activation is reduced in the presence of exogenous rhGas6. ***a–c***, Purified rat microglia were incubated with or without 1 μg/ml LPS for 48 h, and mRNA was measured using qPCR. ***a***, Levels of mRNA of both *CDIIb* and *TNFα*, markers of microglial activation, increased in response to LPS treatment (**$p < 0.01$). ***b***, Expression of both *Axl* and *Mer* mRNA increased in response to LPS-induced activation of microglia (**$p < 0.01$). ***c***, In contrast, expression profiles of both *Tyro3* and *Gas6* mRNA in LPS-activated microglia were not significantly different from control cells ($p > 0.05$). ***d***, Purified rat microglia were cultured in the presence or absence of rhGas6 for 3 h before activation was induced with LPS (1 ng/ml). Cells were harvested after 5 h of LPS treatment and RNA collected. Levels of *TNFα* mRNA, used as a surrogate marker for microglial activation, were measured by qPCR. There was a significant reduction in *TNFα* expression in rhGas6 treated microglia compared with microglia not treated with rhGas6 (**$p < 0.01$, ***$p < 0.001$).

double-label immunohistochemistry for IBA1, a microglial marker, and either Axl or Mer. In contrast to the Tyro3 expression pattern in unchallenged mice, very few Axl-immunoreactive (Fig. 4*a*) or Mer-immunoreactive (Fig. 4*b*) cells were observed in the midline corpus callosum. At this time point, few IBA1-positive cells were observed (Fig. 4*a*,*b*). As expected, an increase in the number of IBA1-positive microglia was detected in the corpus callosum after cuprizone challenge, although numbers were minimally increased after 2 weeks of challenge in the region studied (Fig. 4*c–f*). We found that the vast majority of Axl-positive (Fig. 4*g–k*) and Mer-positive (Fig. 4*h–l*) cells also expressed IBA1, indicating that microglia are the major source of Axl and Mer expression during cuprizone challenge. Additionally, there also appeared to be a dissociation between the expression pattern of Axl and Mer. The immunoreactivity of Axl was more widespread than that of Mer and extended throughout the region of IBA1 reactivity. In contrast, Mer expression appeared restricted to a subset of IBA1-positive microglia.

Activation of microglia alters TAM receptor expression

Because the expression data showed that the upregulation of Axl, Mer, and Gas6 during cuprizone challenge coincided with the activity of microglia, we examined the expression of all three receptors and of Gas6 in microglia *in vitro* under both resting and activated conditions. We cultured purified microglia from postnatal rat cortex in the absence or presence of lipopolysaccharide (LPS) to induce activity. We first confirmed activation of the microglia by assessing the expression of genes encoding two markers of activated microglia, namely *TNFα* and *CD11b* and established that transcripts for both *TNFα* and *CD11b* were significantly increased after LPS stimulation (4.6-fold and 11.5-fold, respectively; $p < 0.01$) (Fig. 5*a*). Microglia activated with LPS also demonstrated increases in both *Axl* and *Mer* gene expression (2.8-fold and 5.2-fold, respectively; $p < 0.01$), compared with unchallenged cells. In contrast, the expression profiles of the *Tyro3* and *Gas6* genes were reduced in the presence of LPS (1.3-fold and 1.5-fold, respectively), although the reduction in expression did not reach significance ($p > 0.05$). These expression patterns exhibited similarities to those identified *in vivo* under demyelinating conditions, although the downregulation of *Tyro3* was not as overt, and the expression of Gas6 was increased after cuprizone challenge (Fig. 2).

We next examined the influence of Gas6 on microglial activation and proliferation. As expected, microglia cultured in the presence of LPS showed a significant increase in the expression of *TNFα* mRNA (Fig. 5*d*) ($p < 0.001$). However, when microglia were treated with rhGas6 and then activated with LPS for 5 h, there was a significant reduction in *TNFα* gene expression compared with microglia treated with LPS alone (Fig. 5*d*) ($p < 0.01$). The expression of *CD11b* was likewise reduced (2.3-fold decrease; $p = 0.0003$) (supplemental Fig. 2, available at www.jneurosci.org as supplemental material). In contrast, in the presence of LPS, Gas6 induced a small but statistically significant increase in the expression of the *IL1β* (1.4-fold increase; $p = 0.01$) and *iNOS* (1.4-fold increase; $p = 0.02$) genes. These data indicate that treatment of microglia with Gas6 can influence the subsequent level of microglial activation induced by LPS. However, the effect of Gas6 on microglia is selective for some signaling pathways, such as that for TNFα, and does not involve a generalized reduction in microglial metabolism. In addition to the effects of Gas6 on microglial activity, in LPS-activated microglia, the expression profiles of *Axl* (1.5-fold increase; $p = 0.06$) and *Mer* (1.7-fold increase; $p = 0.04$) were increased in response to Gas6 (supplemental Fig. 2, available at www.jneurosci.org as supplemental material), potentially increasing the responsiveness of these cells to Gas6 in an autocrine manner.

In addition to the short-term effects of Gas6 on microglial expression, we undertook proliferation studies to determine whether Gas6 affects the mitogenic activity of these cells. We found that after 48 h of treatment with Gas6, there was a strong trend toward a reduction in proliferation in the presence of Gas6 (41.4 ± 4.5 vs 25.5 ± 2.6% BrdU+ cells in the absence or presence of Gas6, respectively; $p = 0.08$). These data indicate that Gas6 could also potentially influence the activity of microglia by reducing the proliferation of these cells.

Demyelination is increased in Gas6$^{-/-}$ mice

We next examined the effect of administering cuprizone to mice lacking expression of Gas6 (Angelillo-Scherrer et al., 2001). Both wild-type and Gas6$^{-/-}$ mice were fed 0.2% cuprizone in chow (w/w) for 3 weeks. The myelin lost among the two genotypes was compared using LFB staining and image analysis as described in Materials and Methods. For analysis of myelination, the corpus callosum was divided by length into three equal segments: rostral, middle, and caudal (outlined in Fig. 6*a*). In all segments and in total, we found no significant difference in the baseline levels of myelination between Gas6$^{-/-}$ and wild-type mice ($p > 0.05$). After 3 weeks of cuprizone challenge, however, myelination levels were significantly reduced in all segments, regardless of genotype (for total corpus callosum, $p = 0.0006$) (Fig. 6*e*). Additionally, a

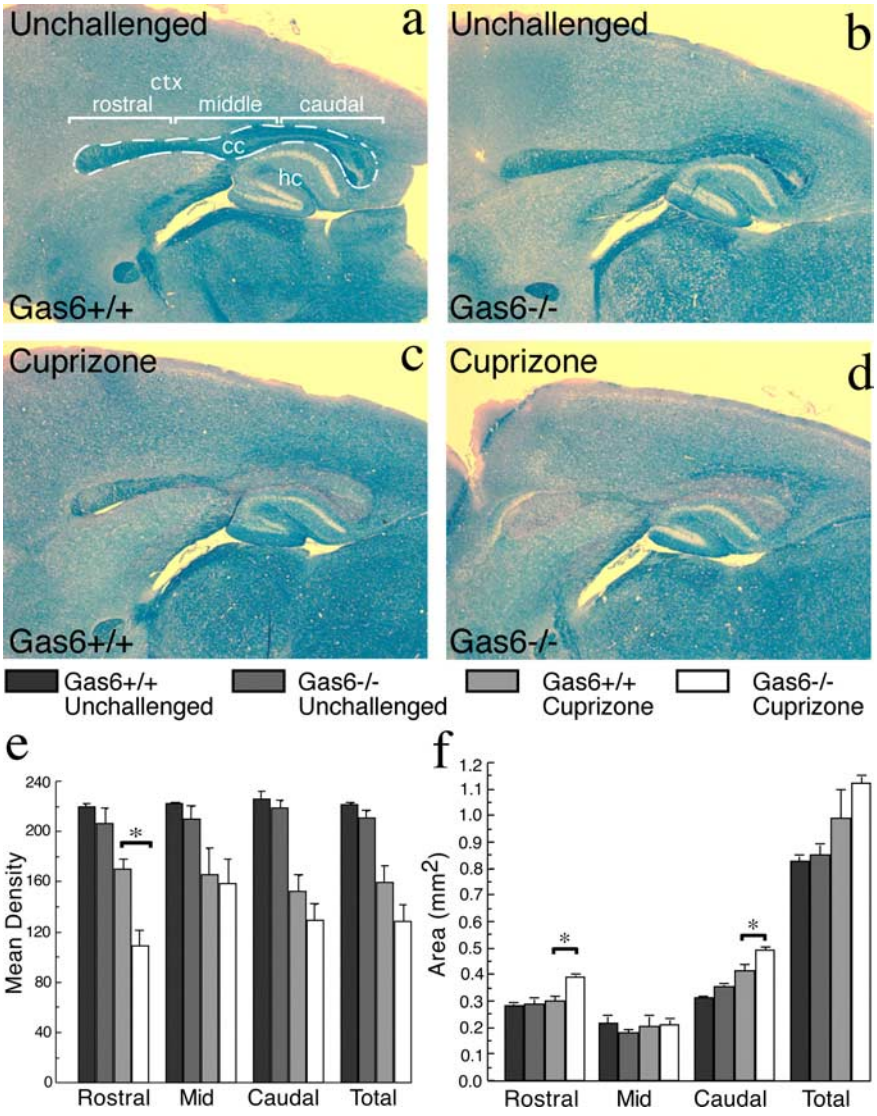

Figure 6. Gas6 $^{-/-}$ mice have decreased myelination and increased callosal area in response to cuprizone challenge. ***a–d***, Wild-type and Gas6 $^{-/-}$ mice were challenged with cuprizone for 3 weeks with age-matched unchallenged mice included as controls ($n = 2$, 3 mice per group). Sagittal sections were assessed using LFB staining with image analysis as described in Materials and Methods. ***e***, A statistically significant decrease in LFB mean density was seen in the rostral segment of Gas6 $^{-/-}$ animals challenged with cuprizone compared with similarly treated wild-type mice (*$p < 0.05$). ***f***, The rostral segment also showed a statistically significant increase in area in Gas6 $^{-/-}$ challenged with cuprizone (*$p < 0.05$). Additionally, there was a significant increase in area of the caudal segment of the corpus callosum in Gas6 $^{-/-}$ mice (*$p < 0.05$). Scale bar, 100 μm. The dotted line indicates the boundaries of the corpus callosum (cc). ctx, Cortex; hc, hippocampus.

significant effect of genotype was observed in the rostral segment of the corpus callosum, where challenged Gas6 $^{-/-}$ mice were significantly demyelinated compared with challenged wild-type mice ($p < 0.05$) (Fig. 6*e*).

In addition to the decrease in myelin density, an increase in the total area of the corpus callosum was identified. Cuprizone-challenged animals showed an overall increase in the area of the corpus callosum, regardless of genotype ($p = 0.0059$) (Fig. 6*f*). The caudal segment of the corpus callosum, where the majority of macrophage/microglia infiltration is seen in cuprizone challenge (Stidworthy et al., 2003), showed a significant increase in area for both wild-type and Gas6 $^{-/-}$ mice with cuprizone challenge ($p = 0.0002$) (Fig. 6*f*). There was also an effect of genotype in the caudal region with the challenged Gas6 $^{-/-}$ mice showing a significant increase in area compared with challenged wild-type mice ($p < 0.05$) (Fig. 6*f*). Unexpectedly, the rostral region of the corpus callosum of Gas6 $^{-/-}$ mice also showed an increase in area compared with either unchallenged mice or challenged wild-type mice ($p < 0.05$) (Fig. 6*f*). This area is typically minimally affected by infiltrating microglia/macrophages in the context of cuprizone challenge in wild-type mice (Stidworthy et al., 2003). An independent cohort of mice was subjected to the same experimental paradigm and analyzed in the coronal plane. The same significant changes in myelin density and callosal area were observed (data not shown).

To analyze in greater detail the loss of myelin shown using LFB staining, the ultrastructure of the rostral segment of the corpus callosum of both wild-type and Gas6 $^{-/-}$ mice either unchallenged or challenged with cuprizone for 3 weeks was examined using electron microscopy. Both unchallenged wild-type and Gas6 $^{-/-}$ mice exhibited a normal complement of healthy axons surrounded by compacted myelin (Fig. 7, *a* and *b*, respectively). Wild-type mice challenged with cuprizone showed a clear reduction in the number of myelinated axons, although some myelinated axons still remained (Fig. 7*c*). In comparison, Gas6 $^{-/-}$ mice showed a severe reduction in the number of myelinated axons, with very few axons appearing to be myelinated to any detectible extent (Fig. 7*d*). To quantify this reduction, semithin sections of the rostral segment of the corpus callosum were stained with methylene blue, and the number of myelinated axons per squared millimeter was determined for each animal (Fig. 7*e*). The number of myelinated axons in the unchallenged state was not significantly different between genotypes ($p > 0.05$). In contrast, cuprizone-challenged Gas6 $^{-/-}$ mice showed a significant reduction in the number of myelinated axons compared with similarly challenged wild-type mice ($p = 0.017$).

Oligodendrocyte numbers are reduced in Gas6 $^{-/-}$ mice in response to cuprizone

Given the data indicating an overall loss of myelin and a reduction in the number of myelinated axons in Gas6 $^{-/-}$ cuprizone-challenged mice compared with their wild-type counterparts, we next examined whether this correlated with a reduction in oligodendrocyte numbers. Coronal sections from cohort 1 were stained with anti-Gst-π, and the number of positive cells in both the rostral and caudal segments of the corpus callosum was determined. No significant difference in the number of Gst-π-positive cells was seen in the unchallenged condition in either the rostral or caudal segments of the corpus callosum of wild-type and Gas6 $^{-/-}$ mice (Fig. 8) ($p > 0.05$). In contrast, Gas6 $^{-/-}$ mice challenged with cuprizone for 3 weeks showed a significant reduction in the number of Gst-π-positive cells compared with similarly challenged wild-type mice in both the rostral (608.4 $\pm$ 96.6 vs 272.6 $\pm$ 32.3 cells/mm^2 for wild-type and Gas6 $^{-/-}$ mice,

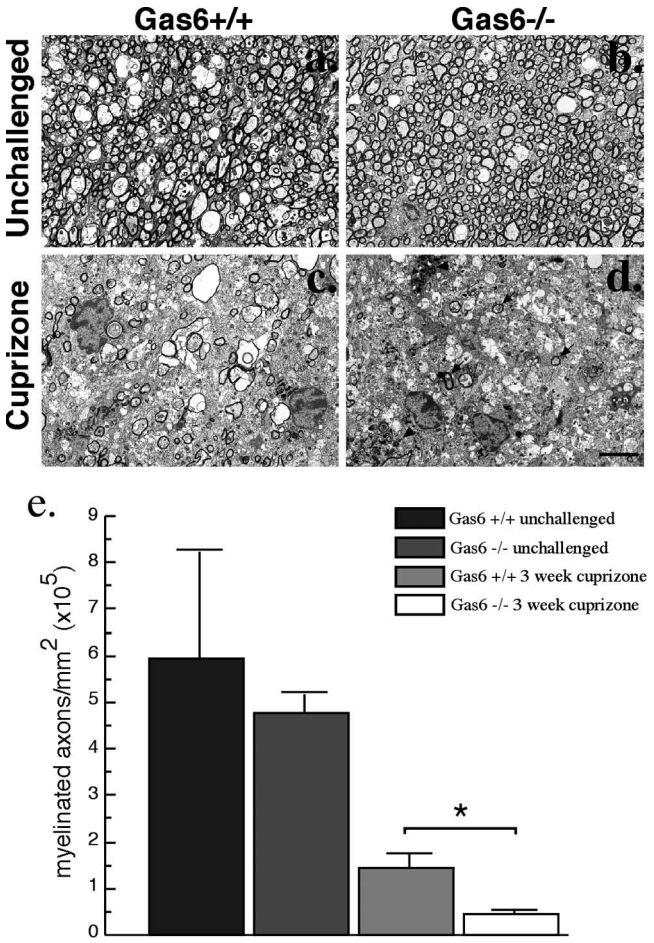

Figure 7. Gas6 $^{-/-}$ mice have reduced numbers of myelinated axons in response to cuprizone challenge. Wild-type and Gas6 $^{-/-}$ mice were challenged with cuprizone for 3 weeks with age-matched unchallenged mice included as controls ($n = 2$, 4 mice per group). ***a–d***, Representative electron micrographs of the rostral segment of the corpus callosum. Unchallenged wild-type (***a***) and Gas6 $^{-/-}$ (***b***) animals show a large number of healthy axons surrounded by compacted myelin. Cuprizone-challenged wild-type (***c***) and Gas6 $^{-/-}$ (***d***) mice show reduced numbers of myelinated axons, with very few remaining in the Gas6 $^{-/-}$ mice. Arrows indicate examples of myelinated axons, and arrowheads indicate examples of microglia with myelin debris. Scale bar, 2 μm. ***e***, Semithin sections from within the rostral segment of the corpus callosum were stained with methylene blue, and the number of myelinated axons within this region was counted. No significant difference in the number of myelinated axons was seen in unchallenged mice ($p > 0.05$). In contrast, compared with their wild-type counterparts, Gas6 $^{-/-}$ mice showed a significant reduction in the number of myelinated axons after cuprizone challenge (*$p < 0.05$).

respectively; $p < 0.01$) and caudal (372.8 ± 99.2 vs 100.6 ± 20.6 cells/mm^2 for wild-type and Gas6 $^{-/-}$ mice, respectively; $p < 0.05$) segments. Consistent with an overall greater loss of myelin in the caudal region, the loss of Gst-π-positive oligodendrocytes was more profound in both genotypes in the caudal segment, equating to a reduction of 70.5% (wild type) and 92.1% (Gas6 $^{-/-}$) in Gst-π-positive oligodendrocytes. Also consistent with our myelin analysis, the difference between genotypes in the loss of Gst-π-positive oligodendrocytes was greater in the rostral segment (51.6% in wild-type mice vs 82.5% in Gas6 $^{-/-}$ mice). These results have been corroborated in an independent cohort in which a statistically significant reduction in oligodendrocyte numbers has been observed within both the corpus callosum and cortex of cuprizone-challenged Gas6 $^{-/-}$ mice compared with their wild-type counterparts (data not shown).

Microglial activity is increased in Gas6 KO mice challenged with cuprizone

We next examined the effect that Gas6 deficiency had on the activation/proliferation of microglia in mice subjected to cuprizone challenge. The number of microglia was determined by staining for the microglial marker IBA1, which is expressed exclusively by microglial/macrophage lineage cells and is increased in response to activation (Ito et al., 1998; Sasaki et al., 2001). As for the analysis of myelination, the corpus callosum was divided by length into three equal segments (rostral, middle, and caudal), and the density of IBA1 staining was assessed as described in Materials and Methods. A significant increase in the level of IBA1 in the rostral segment of Gas6 $^{-/-}$ mice compared with wild-type mice was identified ($p < 0.05$) (Fig. 9*e*). This result was further supported by quantification of the number of IBA1-positive cells in the rostral segment of the corpus callosum. As expected, there was no significant difference between genotypes in the number of IBA1-immunoreactive cells in the unchallenged state (Gas6 $^{-/-}$ 123.5 ± 47.5 cells/mm^2 vs wild-type 30.9 ± 30.9 cells/mm^2; $p > 0.05$) (Fig. 9*f*). Cuprizone-challenged animals, however, showed a significant increase in the number of IBA1-positive cells, regardless of genotype ($p = 0.0091$). Additionally, Gas6 $^{-/-}$ mice challenged with cuprizone showed a significantly increased number of IBA1-positive cells compared with similarly challenged wild-type mice (4696.6 ± 951.8 cells/mm^2 vs 1234 ± 596.7 cells/mm^2, respectively; $p < 0.05$) (Fig. 9*f*). In contrast to the rostral corpus callosum, quantification of cell number in regions other than the rostral corpus callosum, in particular the caudal corpus callosum, although showing a significant increase in microglial numbers in cuprizone-challenged mice, did not show a significant difference between wild-type and Gas6 $^{-/-}$ mice (data now shown).

Discussion

In this study, we have shown that Gas6 is important for the regulation of both myelination and microglial activation in the context of a demyelinating insult, induced by cuprizone. An influence on myelination was demonstrated by reduced levels of LFB staining and a reduction in the number of myelinated axons in Gas6 $^{-/-}$ mice. Numbers of oligodendrocytes were also reduced in Gas6 $^{-/-}$ cuprizone-challenged mice, mirroring an *in vitro* oligodendrocyte survival effect induced by exogenous Gas6. In contrast, the absence of Gas6 led to an increase in the accumulation of microglia/macrophages in response to cuprizone challenge, mirroring the capacity of Gas6 to reduce microglial activation *in vitro*. Collectively, these data demonstrate that Gas6 and the TAM receptors potentially play an important role in both modulating oligodendrocyte survival and microglial activation during demyelination.

Oligodendrocyte death has been shown to be an early event in demyelinating diseases such as multiple sclerosis (Barnett and Prineas, 2004). Previous work in our laboratory has demonstrated that the cytokine LIF can support the survival of oligodendrocytes in cuprizone-mediated demyelination (Emery et al., 2006), and that the provision of either LIF or other similarly acting trophic factors could provide a cogent mechanism for limiting damage during demyelination (Butzkueven et al., 2002, 2006; Marriott et al., 2008). Our *in vitro* data indicate that exogenous Gas6 can also support purified rat oligodendroglial lineage cells. This influence appears restricted to survival effects, given that Gas6 did not act as a mitogen for purified rat oligodendrocyte precursor cells, consistent with the findings of Shankar et al. (2003), who focused on human cells. We have also shown that in

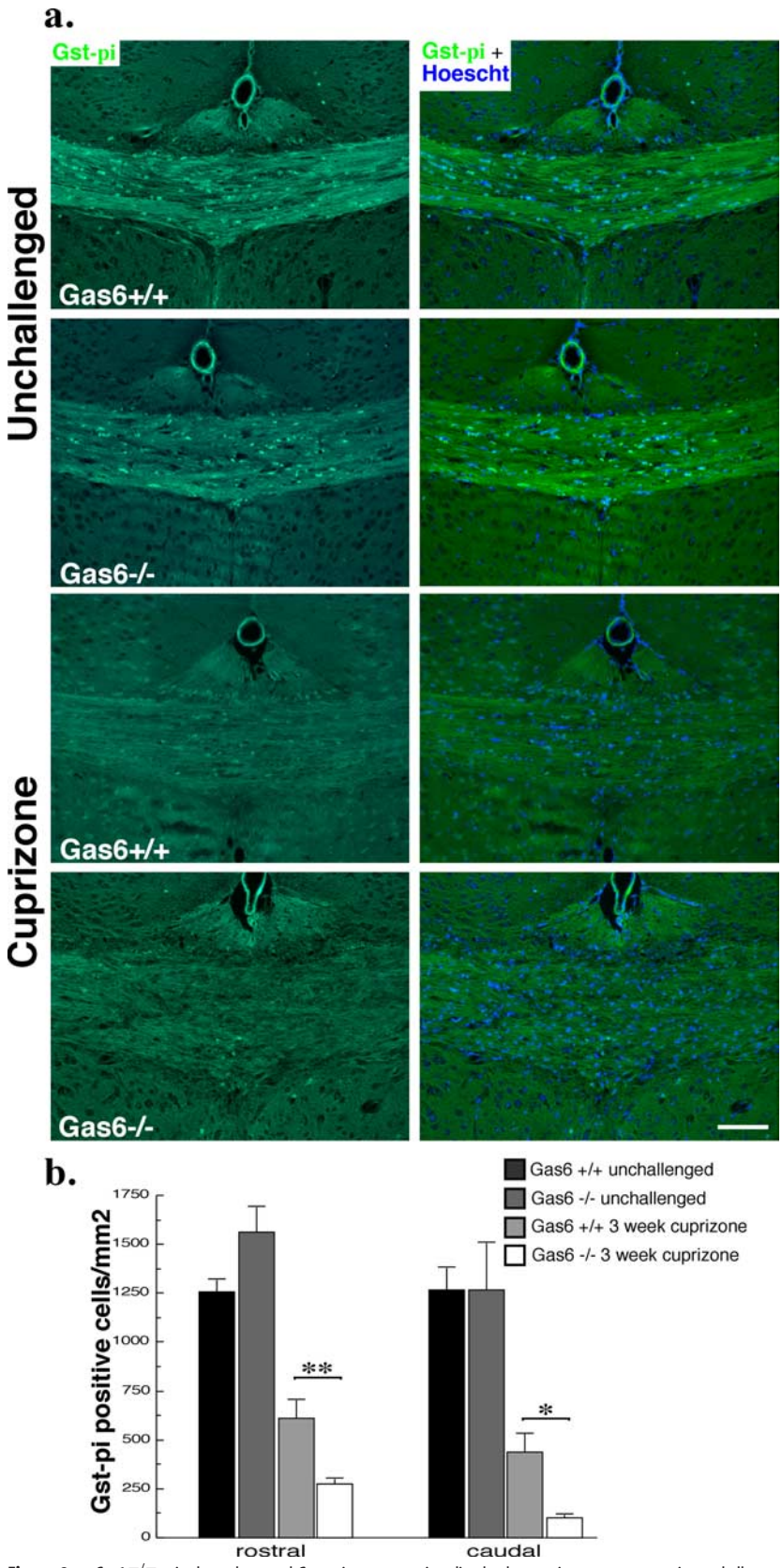

Figure 8. Gas6 $^{-/-}$ mice have decreased Gst-π-immunoreactive oligodendrocytes in response to cuprizone challenge. Wild-type and Gas6 $^{-/-}$ mice were challenged with cuprizone for 3 weeks with age-matched unchallenged mice included as controls ($n = 3, 5$ for each group). Immunofluorescence analysis was performed to detect the presence of Gst-π reactive oligodendrocytes. ***a***, Representative images of Gst-π staining and the same image merged with the nuclear stain Hoescht are shown. Scale bar, 100 μm. The number of Gst-π-positive cells per squared millimeter was determined as outlined in Materials and Methods, and the results are shown in ***b***, with Gas6 $^{-/-}$ mice showing a significant decrease in oligodendrocytes in both the rostral and caudal segments of the corpus callosum. *$p < 0.05$, **$p < 0.01$.

the absence of Gas6 *in vivo*, the extent of demyelination in response to 3 weeks of cuprizone challenge is increased, and that the number of Gst-π-positive oligodendrocytes is reduced. These data suggest that Gas6 could play an important role in promoting mature oligodendrocyte survival *in vivo* during a demyelinating event. In addition, our data provide strong circumstantial evidence for a direct effect of Gas6 on oligodendrocytes. This is posited, because the loss of Gst-π-positive oligodendrocytes was increased by Gas6 deficiency in the absence of increased microglial numbers within the caudal corpus callosum and within the cerebral cortex of cuprizone-challenged mice.

Which of the TAM receptors could be responsible for mediating such an oligodendrocyte-specific effect? Prieto et al. (2000, 2007) have reported that Tyro3 protein is expressed by oligodendrocytes in the healthy adult rodent brain. In addition, we found that the expression of the Tyro3 gene is negatively correlated with the damage/death of oligodendrocytes over the course of cuprizone-induced demyelination. We have also shown that CNPase-positive oligodendrocytes within the healthy mouse corpus callosum express Tyro3 protein. It is therefore possible that Gas6 could act through Tyro3 early after cuprizone challenge to delay oligodendrocyte injury, but that this effect is lost with time and that with additional damage, loss of Tyro3 receptor expression results in decreased responsiveness to Gas6. In contrast, previous *in vitro* studies assessing oligodendrocytes isolated from wild-type and Axl knock-out mice have also indicated a role for this receptor in the maintenance of oligodendrocyte viability (Shankar et al., 2006).

Microglial proliferation and accumulation are early responses to cuprizone and peak at ~4–5 weeks of challenge (Blakemore, 1972; Hiremath et al., 1998). Activated microglia secrete a variety of proteins, including cytokines and reactive oxygen species, which can ultimately lead to oligodendrocyte damage. Microglia can also secrete trophic factors, which could support damaged cells and induce repair. *In vitro* studies have demonstrated that microglia can either be directly toxic to oligodendrocytes (Nicholas et al., 2003; Li et al., 2005) or can support oligodendrocyte survival (Pang et al., 2000; Nicholas et al., 2001, 2002), with the predominant effect being context dependant. Dichotomous effects of microglia also appear to occur *in vivo* with reports of either deleterious (McMahon et al., 2001; Mana et al., 2006; Pasquini et al., 2007) or protective effects in response to cuprizone-induced demyelination, the latter particularly predominant during the remyelination phase (Arnett et al., 2001, 2002, 2003).

Our results show a correlation between the level of microglial activation/accumulation and increased demyelination in response to cupri-

zone. Furthermore, the expression of both Axl and Mer not only increase over the course of cuprizone challenge, in a temporal profile similar to that of the microglial accumulation and activation, double-immunohistochemical staining demonstrated that the majority of both Axl and Mer expressing cells were IBA1-positive microglia. These data argue strongly that this component part of Gas6 signaling via Axl and Mer is likely to be mediated directly, at least in part, via microglia. Previous work from other laboratories has shown that exogenous Gas6 can induce the expression of Twist1, the expression of which can lead to suppression of the cytotoxic cytokine TNFα in cultured human macrophages (Sharif et al., 2006). Our *in vitro* data, demonstrating upregulated expression of Axl and Mer transcripts and downregulation *TNFα* transcripts in purified microglia in response to Gas6, provide the first direct evidence that TAM receptor signaling can downregulate a deleterious microglial response. Supportive of this view, both Axl and Mer have also been shown previously to transduce signals in peripheral macrophages (Camenisch et al., 1999; Scott et al., 2001; Sharif et al., 2006). Mer has also been shown to be involved in regulating the response of macrophages *in vivo* to lipopolysaccharide treatment, with Mer knock-out mice more susceptible to death from endotoxic shock because of an overproduction of TNFα by macrophages (Camenisch et al., 1999).

Given the known role that the TAM receptors play in regulating the immune response (for review, see Lemke and Lu, 2003), it seems likely that in the absence of Gas6, the microglia could fail to receive signals to return to a resting phenotype. In the cuprizone model, this chronic activation of microglia could potentially contribute to damage to oligodendrocytes and enhanced demyelination, although as indicated above our data, generated from the caudal corpus callosum and cortex, could be interpreted to argue for an independent oligodendrocyte-specific effect. It should be noted, however, that even in these regions, the millieu of cytokines produced by microglia could be influenced by Gas6, independent of an influence on their numbers. Furthermore, in some cases of multiple sclerosis, microglial activation has been observed to precede the loss of myelin, indicating that microglial activation is not always a simple response mechanism (Barnett and Prineas, 2004). It is also possible that the variable expression profiles of the TAM receptors in the context of demyelination, with Axl and Mer rather than Tyro3 being shown to be expressed by microglia, could indicate cell lineage-specific roles for each of the family members. The study of cuprizone-induced demyelination of TAM receptor single knock-out mice, including animals in which the receptors are conditionally deleted by selected cell lineages, could therefore assist in dissecting out specific influences on microglial activation and oligodendrocyte loss and in identifying the molecular pathways responsible for mediating these effects.

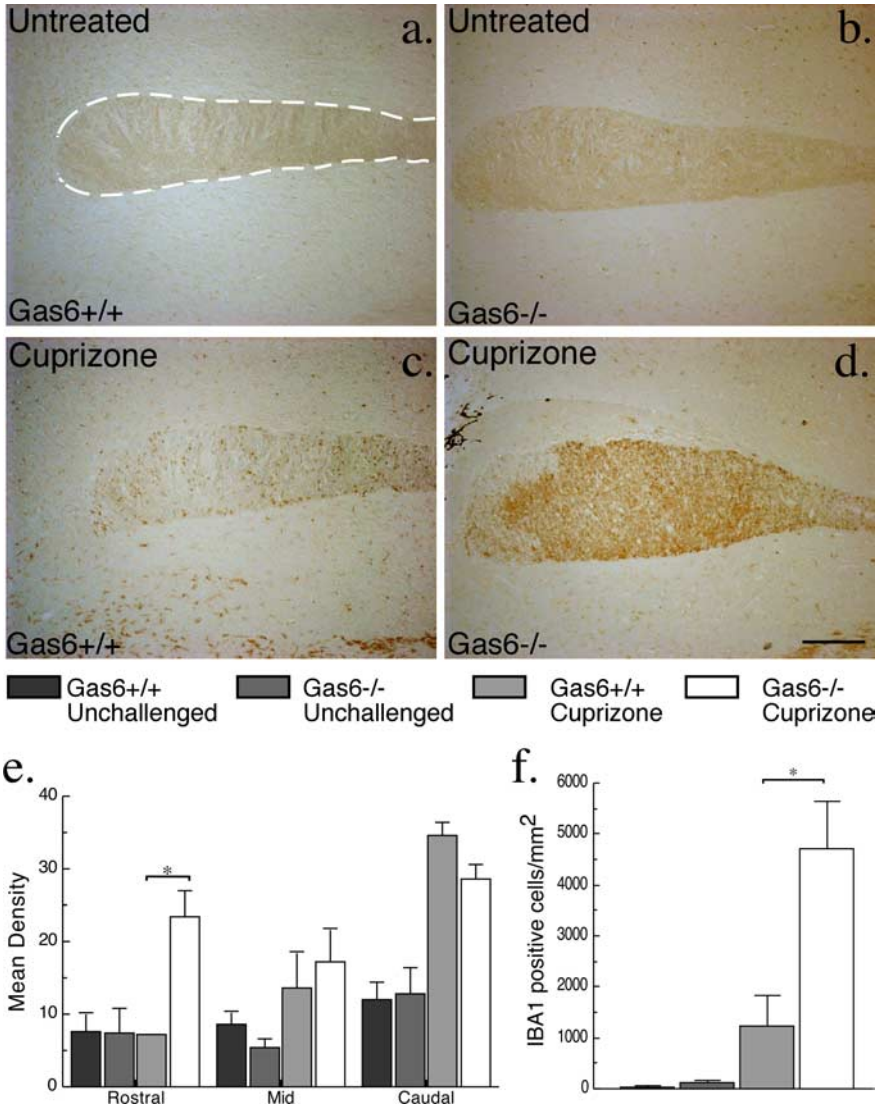

Figure 9. Gas6$^{-/-}$ mice have an increased number of IBA1-positive microglia/macrophages in the rostral corpus callosum in response to cuprizone challenge. Wild-type and Gas6$^{-/-}$ mice were challenged with cuprizone for 3 weeks with age-matched unchallenged mice included as controls ($n = 2, 3$ for each group). Immunohistochemistry was performed to detect the presence of IBA1 reactive microglia/macrophages. ***a–d***, Representative images of the rostral segment of the corpus callosum are shown for each condition. The dotted line indicates the boundaries of the corpus callosum. Scale bar, 200 μm. The corpus callosum was divided into three separate segments, and the mean density of staining was determined as outlined in Materials and Methods. The results are shown in ***e***, with Gas6$^{-/-}$ mice showing an increase in IBA1 staining density in the rostral segment (*$p < 0.05$). ***f***, Adjacent sections were stained with IBA1 and counterstained with hemotoxylin to enable counting of individual cells in the rostral segment. No significant difference in the number of IBA1-positive cells was seen in unchallenged mice. In contrast, a significant increase in the number of IBA1-positive cells was observed in the cuprizone-challenged Gas6$^{-/-}$ mice compared with their wild-type counterparts (*$p < 0.05$).

The results presented in this study indicate an important role for TAM receptor signaling in modulating the response of both oligodendrocytes and microglia to cuprizone-induced demyelination. In the absence of Gas6 signaling, microglial activation is potentiated, oligodendrocyte numbers are reduced, and demyelination is increased. Additional work is required to formally resolve which of the effects are a direct result of loss of Gas6 signaling and which, if any, are secondary. It will also be important to determine whether Gas6 signaling is a crucial factor in promoting

oligodendrocyte–microglial interactions. Independent of this, we have established the importance of TAM receptors as potential novel therapeutic targets for the treatment of demyelinating disease.

References

Angelillo-Scherrer A, de Frutos P, Aparicio C, Melis E, Savi P, Lupu F, Arnout J, Dewerchin M, Hoylaerts M, Herbert J, Collen D, Dahlback B, Carmeliet P (2001) Deficiency or inhibition of Gas6 causes platelet dysfunction and protects mice against thrombosis. Nat Med 7:215–221.

Arnett HA, Mason J, Marino M, Suzuki K, Matsushima GK, Ting JP (2001) TNF alpha promotes proliferation of oligodendrocyte progenitors and remyelination. Nat Neurosci 4:1116–1122.

Arnett HA, Hellendall RP, Matsushima GK, Suzuki K, Laubach VE, Sherman P, Ting JP (2002) The protective role of nitric oxide in a neurotoxicant-induced demyelinating model. J Immunol 168:427–433.

Arnett HA, Wang Y, Matsushima GK, Suzuki K, Ting JP (2003) Functional genomic analysis of remyelination reveals importance of inflammation in oligodendrocyte regeneration. J Neurosci 23:9824–9832.

Barnett MH, Prineas JW (2004) Relapsing and remitting multiple sclerosis: pathology of the newly forming lesion. Ann Neurol 55:458–468.

Barres BA, Hart IK, Coles HS, Burne JF, Voyvodic JT, Richardson WD, Raff MC (1992) Cell death and control of cell survival in the oligodendrocyte lineage. Cell 70:31–46.

Barres BA, Schmid R, Sendnter M, Raff MC (1993) Multiple extracellular signals are required for long-term oligodendrocyte survival. Development 118:283–295.

Blakemore WF (1972) Observations on oligodendrocyte degeneration, the resolution of status spongiosus and remyelination in cuprizone intoxication in mice. J Neurocytol 1:413–426.

Bottenstein JE, Sato GH (1979) Growth of a rat neuroblastoma cell line in serum-free supplemented medium. Proc Natl Acad Sci USA 76:514–517.

Butzkueven H, Zhang JG, Soilu-Hanninen M, Hochrein H, Chionh F, Shipham KA, Emery B, Turnley AM, Petratos S, Ernst M, Bartlett PF, Kilpatrick TJ (2002) LIF receptor signaling limits immune-mediated demyelination by enhancing oligodendrocyte survival. Nat Med 8:613–619.

Butzkueven H, Emery B, Cipriani T, Marriott MP, Kilpatrick TJ (2006) Endogenous leukemia inhibitory factor production limits autoimmune demyelination and oligodendrocyte loss. Glia 53:696–703.

Camenisch TD, Koller BH, Earp HS, Matsushima GK (1999) A novel receptor tyrosine kinase, Mer, inhibits TNF-alpha production and lipopolysaccharide-induced endotoxic shock. J Immunol 162:3498–3503.

Emery B, Cate HS, Marriott M, Merson T, Binder MD, Snell C, Soo PY, Murray S, Croker B, Zhang JG, Alexander WS, Cooper H, Butzkueven H, Kilpatrick TJ (2006) Suppressor of cytokine signaling 3 limits protection of leukemia inhibitory factor receptor signaling against central demyelination. Proc Natl Acad Sci USA 103:7859–7864.

Hiremath MM, Saito Y, Knapp GW, Ting JP, Suzuki K, Matsushima GK (1998) Microglial/macrophage accumulation during cuprizone-induced demyelination in C57BL/6 mice. J Neuroimmunol 92:38–49.

Ito D, Imai Y, Ohsawa K, Nakajima K, Fukuuchi Y, Kohsaka S (1998) Microglia-specific localisation of a novel calcium binding protein, Iba1. Brain Res Mol Brain Res 57:1–9.

Lai C, Lemke G (1991) An extended family of protein-tyrosine kinase genes differentially expressed in the vertebrate nervous system. Neuron 6:691–704.

Lemke G, Lu Q (2003) Macrophage regulation by Tyro 3 family receptors. Curr Opin Immunol 15:31–36.

Li J, Lin JC, Wang H, Peterson JW, Furie BC, Furie B, Booth SL, Volpe JJ, Rosenberg PA (2003) Novel role of vitamin K in preventing oxidative injury to developing oligodendrocytes and neurons. J Neurosci 23:5816–5826.

Li J, Baud O, Vartanian T, Volpe JJ, Rosenberg PA (2005) Peroxynitrite generated by inducible nitric oxide synthase and NADPH oxidase mediates microglial toxicity to oligodendrocytes. Proc Natl Acad Sci USA 102:9936–9941.

Li R, Chen J, Hammonds G, Phillips H, Armanini M, Wood P, Bunge R, Godowski PJ, Sliwkowski MX, Mather JP (1996) Identification of Gas6 as a growth factor for human Schwann cells. J Neurosci 16:2012–2019.

Livak KJ, Schmittgen TD (2001) Analysis of relative gene expression data using real-time quantitative PCR and the 2(-Delta Delta C(T)) method. Methods 25:402–408.

Lu Q, Lemke G (2001) Homeostatic regulation of the immune system by receptor tyrosine kinases of the Tyro 3 family. Science 293:306–311.

Lu Q, Gore M, Zhang Q, Camenisch T, Boast S, Casagranda F, Lai C, Skinner MK, Klein R, Matsushima GK, Earp HS, Goff SP, Lemke G (1999) Tyro-3 family receptors are essential regulators of mammalian spermatogenesis. Nature 398:723–728.

Mana P, Linares D, Fordham S, Staykova M, Willenborg D (2006) Deleterious role of IFNgamma in a toxic model of central nervous system demyelination. Am J Pathol 168:1464–1473.

Marriott M, Emery B, Cate H, Binder M, Kemper D, Wu Q, Kolbe S, Gordon I, Wang H, Egan G, Murray S, Butzkueven H, Kilpatrick TJ (2008) Leukemia inhibitory factor signalling modulates both central nervous system demyelination and myelin repair. Glia 56:686–698.

Matsushima GK, Morell P (2001) The neurotoxicant, cuprizone, as a model to study demyelination and remyelination in the central nervous system. Brain Pathol 11:107–116.

McCarthy KD, de Vellis J (1980) Preparation of separate astroglial and oligodendroglial cell cultures from rat cerebral tissue. J Cell Biol 85:890–902.

McMahon EJ, Cook DN, Suzuki K, Matsushima GK (2001) Absence of macrophage-inflammatory protein-1alpha delays central nervous system demyelination in the presence of an intact blood-brain barrier. J Immunol 167:2964–2971.

McMahon EJ, Suzuki K, Matsushima GK (2002) Peripheral macrophage recruitment in cuprizone-induced CNS demyelination despite an intact blood-brain barrier. J Neuroimmunol 130:32–45.

Nagata K, Ohashi K, Nakano T, Arita H, Zong C, Hanafusa H, Mizuno K (1996) Identification of the product of growth arrest-specific gene 6 as a common ligand for Axl, Sky, and Mer receptor tyrosine kinases. J Biol Chem 271:30022–30027.

Nicholas R, Stevens S, Wing M, Compston A (2003) Oligodendroglial-derived stress signals recruit microglia in vitro. NeuroReport 14:1001–1005.

Nicholas RS, Wing MG, Compston A (2001) Nonactivated microglia promote oligodendrocyte precursor survival and maturation through the transcription factor NF-kappa B. Eur J Neurosci 13:959–967.

Nicholas RS, Stevens S, Wing MG, Compston DA (2002) Microglia-derived IGF-2 prevents TNFalpha induced death of mature oligodendrocytes in vitro. J Neuroimmunol 124:36–44.

Pang Y, Cai Z, Rhodes PG (2000) Effects of lipopolysaccharide on oligodendrocyte progenitor cells are mediated by astrocytes and microglia. J Neurosci Res 62:510–520.

Pasquini LA, Calatayud CA, Bertone Una AL, Millet V, Pasquini JM, Soto EF (2007) The neurotoxic effect of cuprizone on oligodendrocytes depends on the presence of pro-inflammatory cytokines secreted by microglia. Neurochem Res 32:279–292.

Paxinos G, Franklin KBJ (2001) The mouse brain in stereotaxic coordinates, Ed 2. New York: Elsevier.

Prasad D, Rothlin CV, Burrola P, Burstyn-Cohen T, Lu Q, Garcia de Frutos P, Lemke G (2006) TAM receptor function in the retinal pigment epithelium. Mol Cell Neurosci 33:96–108.

Prieto AL, Weber JL, Lai C (2000) Expression of the receptor protein-tyrosine kinases Tyro-3, Axl, and mer in the developing rat central nervous system. J Comp Neurol 425:295–314.

Prieto AL, O'Dell S, Varnum B, Lai C (2007) Localisation and signaling of the receptor protein tyrosine kinase Tyro-3 in cortical and hippocampal neurons. Neuroscience 150:319–334.

Raivich G, Banati R (2004) Brain microglia and blood-derived macrophages: molecular profiles and functional roles in multiple sclerosis and animal models of autoimmune demyelinating disease. Brain Res Brain Res Rev 46:261–281.

Sasaki Y, Ohsawa K, Kanazawa H, Kohsaka S, Imai Y (2001) Iba1 is an actin-cross-linking protein in macrophages/microglia. Biochem Biophys Res Commun 286:292–297.

Scott RS, McMahon EJ, Pop SM, Reap EA, Caricchio R, Cohen PL, Earp HS, Matsushima GK (2001) Phagocytosis and clearance of apoptotic cells is mediated by MER. Nature 411:207–211.

Shankar SL, O'Guin K, Cammer M, McMorris FA, Stitt TN, Basch RS, Varnum B, Shafit-Zagardo B (2003) The growth arrest-specific gene product Gas6 promotes the survival of human oligodendrocytes via a

phosphatidylinositol 3-kinase-dependent pathway. J Neurosci 23:4208–4218.

Shankar SL, O'Guin K, Kim M, Varnum B, Lemke G, Brosnan CF, Shafit-Zagardo B (2006) Gas6/Axl signaling activates the phosphatidylinositol 3-kinase/Akt1 survival pathway to protect oligodendrocytes from tumor necrosis factor alpha-induced apoptosis. J Neurosci 26:5638–5648.

Sharif MN, Sosic D, Rothlin CV, Kelly E, Lemke G, Olson EN, Ivashkiv LB (2006) Twist mediates suppression of inflammation by type I IFNs and Axl. J Exp Med 203:1891–1901.

Stidworthy MF, Genoud S, Suter U, Mantei N, Franklin RJ (2003) Quantifying the early stages of remyelination following cuprizone-induced demyelination. Brain Pathol 13:329–339.

Stitt TN, Conn G, Gore M, Lai C, Bruno J, Radziejewski C, Mattsson K, Fisher J, Gies DR, Jones PF, Masiakowski P, Ryan TE, Tobkes NJ, Chen DH, DiStefano PS, Long GL, Basilico C, Goldfarb MP, Lemke G, Glass DJ, et al. (1995) The anticoagulation factor protein S and its relative, Gas6, are ligands for the Tyro 3/Axl family of receptor tyrosine kinases. Cell 80:661–670.

Wang H, Chen Y, Ge Y, Ma P, Ma Q, Ma J, Xue S, Han D (2005) Immunoexpression of Tyro 3 family receptors–Tyro 3, Axl, and Mer–and their ligand Gas6 in postnatal developing mouse testis. J Histochem Cytochem 53:1355–1364.

Yagami T, Ueda K, Asakura K, Sakaeda T, Nakazato H, Kuroda T, Hata S, Sakaguchi G, Itoh N, Nakano T, Kambayashi Y, Tsuzuki H (2002) Gas6 rescues cortical neurons from amyloid beta protein-induced apoptosis. Neuropharmacology 43:1289–1296.